Int. J. Nano Dimens. 2026; 17(1) : 92-105

International Journal of Nano Dimension (IJND)

https://dx.doi.org/10.57647/j.ijnd.2026.1701.06

Original Research

The Capability of Pure and Metal-Encapsulated All Boron Fullerenes (B40) as Nanocarriers for β-Lapachone Anticancer Drug Delivery: DFT Study

Mercedeh Hemmatian[1], Sharieh Hosseini[2,*], Hakimeh Ziyadi[1], Ehsan Shakerzadeh[3], Marjan Jebeli Javan[1]

[1]*Department of Organic Chemistry, TeMS.C., Islamic Azad University, Tehran, Iran*
[2]*Department of Chemistry, TeMS.C., Islamic Azad University, Tehran, Iran*
[3]*Chemistry Department, Faculty of science, Shahid Chamran University of Ahvaz, Ahvaz, Iran*

[*]**Corresponding author:** sh.hosseini@iautmu.ac.ir

Article History

Received:
22 May 2025

Revised:
22 June 2025

Accepted:
8 July 2025

Published online:
30 July 2025

Published in Issue:
2 January 2026

Abstract:

This work employs density functional theory (DFT) to explore the interactions between the anticancer agent β-Lapachone (β-Lap) and pristine B40 fullerenes as well as their potassium- and magnesium-encapsulated counterparts (K@B40 and Mg@B40). The results reveal significant interactions affecting the electronic structures of these molecules, with stable complexes formed and a notable reduction in energy gaps, indicating effective β-Lap adsorption. The β-Lap drug exhibits stronger binding to metal-encapsulated fullerenes than to pristine B40 in both aqueous and gas environments, with binding energies in water of approximately −5.2 kcal/mol for B40, −82.9 kcal/mol for Mg@B40, and −55.7 kcal/mol for K@B40. In aqueous media, the dipole moments of encapsulated complexes rise to nearly twice their gas-phase values. To complement the electronic structure insights, we employ Quantum Theory of Atoms in Molecules (QTAIM) to study the electron densities and their Laplacians, and Natural Bond Orbital (NBO) analysis to evaluate donor–acceptor interactions and charge redistribution within these complexes. Despite the strong adsorption energies, the interaction weakens in acidic conditions, facilitating drug release. These findings suggest that B40 and its metal-encapsulated derivatives are promising nanocarriers for β-Lap delivery, combining strong binding with controlled release potential in biological environments.

Keywords: Adsorption; All boron fullerene; β-Lapachone; DFT calculation; Metal encapsulation

Cite this article: Hemmatian M, Hosseini S, Ziyadi H, Shakerzadeh E, Jebeli Javan M, The Capability of Pure and Metal-Encapsulated All Boron Fullerenes (B40) as Nanocarriers for β-Lapachone Anticancer Drug Delivery: DFT Study. Int. J. Nano Dimens. 2026;17(1): 92-105. https://doi.org/10.57647/j.ijnd.2026.1701.06

1. Introduction

Nanomedicine encompasses the deployment of nanoscale technologies within healthcare [1, 2, 3, 4, 5]. It involves the application of nanomaterials and nanodevices to diagnose, treat, and prevent diseases [6, 7, 8]. The field of nanomedicine covers a broad spectrum of uses, including the deployment of nanoparticles for drug delivery [9, 10, 11, 12, 13, 14], nano biosensors for diagnostics [15], and nanodevices for targeted therapy and theragnostic which combines diagnosis and treatment [8, 16, 17, 18]. Cancer treatment options encompass surgical procedures, radiation therapy, chemotherapy, and targeted therapy [19, 20, 21]. The selection of treatment is typically influenced by the cancer type and stage, along with the patient's general health and personal preferences [22, 23, 24, 25, 26]. Despite numerous advancements in medicine, cancer remains one of the most lethal diseases, highlighting the crucial need for developing new treatment approaches with minimal adverse effects [27, 28, 29, 30, 31, 32, 33]. Fullerene structures and their derivatives are very important owing to their applications in magnetic recording imaging, electronic materials and

devices, environmental processes, drug transport, etc. [34, 35]. Also, their doping with different types of atoms or molecules is of interest [36].

Fullerene, with the ability to carry multiple drug loads and with targeted drug delivery, can eliminate many of the side effects of chemotherapy [37]. It should be noted that so far many nanomaterials have been tested for chemotherapy, but fullerene-based systems stand out as the most favorable options because of their distinct structure and properties [38]. For the first time, Zhai et al. successfully synthesized B40 fullerene [39]. The study revealed that among carbon fullerenes and boron clusters, the B40 cage exhibits the greatest stability, owing to its combination of acidic and basic sites. Structurally, the neutral B40 forms an interwoven double-chain framework, featuring two hexagonal faces at its poles and four heptagonal rings around its equator. Crucially, its almost spherical shape encloses an internal cavity of approximately 6.2 Å in diameter, indicating a strong potential for metal-atom encapsulation [40]. Muath Suliman and colleagues recently showcased through DFT analysis and molecular docking simulation that curcumin-decorated B40 and SiB39 fullerenes exhibit promising capabilities in combating cancer and inflammation [41].

Research has shown that in most cases of encapsulation of metals, especially alkali and alkali metals has increased the reactivity of fullerenes and increased adsorption capacity [42].

Endohedral metallo-borofullerenes offer promising applications in nano chemistry. For instance, entrapping a Li atom inside a B40 cage can substantially boost its CO_2 adsorption capacity [43, 44, 45, 46, 47, 48]. In the other study, by using DFT calculation, demonstrate that B40 and M@B40 fullerene possess a significant capability for absorbing numerous 5-FU molecules efficiently [47]. Also Na and Ca encapsulated B40 increased adsorption of Melphalan on the surface of fullerene [49]. W. Fa et al. examined the stability of B40 when combined with metals such as Li, Ba, Na, and Tl. The studies on the metals, such as thallium, sodium, barium and lithium show that among the mentioned metals, thallium, potassium and lithium like to be placed outside and potassium and barium tend to be placed inside the cage of fullerene [50].

Bai and coworkers exhibited the remarkable stability of Ca and Sr-encapsulated B40 [51]. β-Lap (an ortho-naphthoquinone) isolated from the lapacho tree (Tabebuia avellanedae) in South America [52] has been the focus of extensive research, which has revealed a wide array of biological activities, including antibacterial, antitumor, Trypanosoma cruzi, antimalarial, anti- anti- metabolic-syndrome–modulating, anti-inflammatory and Mycobacterium tuberculosis effects [53, 54, 55, 56]. This natural compound has demonstrated efficacy in combating various forms of cancer, including prostate, lung, pancreatic, and melanoma [57]. This drug has several drawbacks, including uneven distribution, systemic toxicity and limited solubility, when administered parenterally [58]. Aref Gholami and colleagues employed DFT calculations to evaluate both B36N36 and metal-encapsulated B36N36 fullerenes as nanocarriers for the anticancer agent β-Lap. Their results showed that, in both gas and aqueous environments, the metal- encapsulated B36N36 cages exhibit higher binding energies, indicating that metal encapsulation markedly enhances β-Lap adsorption [59]. The purpose of this article is to investigate the possibilities of using pure and metal-encased B40 fullerenes as carrier for β-Lap molecule, representing the initial in-depth study of this topic.

2. Computational details

The quantum mechanical investigations, including geometry optimizations, density of states (DOS) calculations and NBO analyses were carried out on the B40 fullerene, M@B40 (M = Mg and K) and their β-lap/B40 complexes using DFT. All computations employed the B3LYP hybrid exchange–correlation functional together with the 6-31G+(d,p) basis set, a combination well established for accurately modeling a variety of nanostructures [60, 61, 62]. All optimizations and frequency analyses (to confirm the absence of imaginary modes and thus verify true minima) were performed in Gaussian 09 [63]. DOS profiles were generated with the Multiwfn program [64], and from the resulting electronic structures we extracted the lowest unoccupied molecular orbital (LUMO), the highest occupied molecular orbital (HOMO), and the corresponding HOMO–LUMO gap (E_g).

No symmetry constraints were imposed during geometry optimization. Spin multiplicities were set to singlet for Mg@B40 and doublet for K@B40, and all open-shell cases were treated via the unrestricted formalism [65].

Adsorption energies (E_{ads}) of β-lap molecules on Bare B40 and M@B40 is obtained. To rectify the basis set superposition error (BSSE), enhance the electrical stability of the systems, and evaluate the suitable interaction between the β-lap molecule and B40 fullerenes, the following equations are employed:

$$E_{ads} = E_{drug/B40} - (E_{B40} + E_{drug}) + E_{BSSE} \quad (1)$$

$$E_{ads} = E_{drug/Mg@B40} - (E_{Mg@B40} + E_{drug}) + E_{BSSE} \quad (2)$$

$$E_{ads} = E_{drug/K@B40} - (E_{K@B40} + E_{drug}) + E_{BSSE} \quad (3)$$

The adsorption Gibbs free energy (ΔG_{ads}) and enthalpy (ΔH_{ads}) were evaluated at T = 298.15 K and P = 1 atm using the following expressions:

$$\Delta G_{ads} = G_{complex} - (G_{drug} + G_{B40-fullerene}) \quad (4)$$

$$\Delta H_{ads} = H_{complex} - (H_{drug} + H_{B40-fullerene}) \quad (5)$$

Here, $G_{complex}$, G_{drug}, and G_{B40} represent the zero-point–corrected Gibbs free energies of the drug–fullerene adduct, the isolated β-lapachone molecule, and the B40, respectively. Similarly, $H_{complex}$, H_{drug}, and H_{B40} denote their corresponding enthalpies [66].

All adsorption analyses under biologically relevant conditions were performed in an implicit aqueous environment by re-optimizing all structures with the polarizable continuum model (PCM) to mimic water solvation

https://dx.doi.org/10.57647/j.ijnd.2026.1701.06

[66]. The solvation energy (E_{solv}) for each species was then computed as:

$$E_{solv} = E_{hyd} - E_{ads} \quad (6)$$

where E_{solv}, E_{hyd} and E_{ads} are solvation energy, adsorption energy in water media, and adsorption energy in the gas phase respectively. NBO and QTAIM analyses are efficient tools for representing the electron density in numerous systems [67, 68, 69].

NBO analyses were carried out at the B3LYP/6-31+G(d,p) level. This approach quantifies donor–acceptor (bond–anti bond) interactions by evaluating their second-order perturbation stabilization energies (E^2) [70, 71, 72, 73, 74, 75]. These E^2 values were calculated as follows:

$$E^2 = \Delta E_{ij} = q_i \frac{F^2(i,j)}{\varepsilon_j - \varepsilon_i} \quad (7)$$

where, $F(i,j)$ is the off-diagonal part of the NBO Fock matrix, q_i is the orbital occupation of the donor, and ε_i; ε_j are the diagonal components (orbital energies).

QTAIM analysis prepared a potent technique for electron delocalization analysis. The Atomic in Molecule Analysis (AIM) method is also applicable for examining the differences between agostic interactions and hydrogen bonds. Within AIM analysis, the bond interaction characteristics are assessed based on electron density properties. In this framework, the value of electron density $\rho(r)$ at a bond critical point reflects the bond's strength, and the identification of a BCP between two atoms denotes the existence of a bonding interaction. Therefore, to investigate the characteristics of the anchor bond, one can utilize the existence of BCP and the topological properties of $\rho(r)$. A series of guidelines for identifying anchor bonds were suggested primarily on QTAIM [76]. Common standards of the existence of an anchor bond are $\nabla^2\rho(r)$ in BCPs and $\rho(r)$. $\rho(r)$ is related to the bond interaction energy by the local expression of the virial theorem [68]. This parameter is related to the declaration of the viral formula with the bond interaction energy:

$$\left(\frac{\hbar^2}{4m}\right)\nabla^2\rho(r) = 2G(r) + V(r) \quad (8)$$

The electronic energy density at a bond critical point, $H(r)$, is given by the sum of the potential energy densities $V(r)$ and local kinetic $G(r)$ [67]:

$$H(r) = G(r) + V(r) \quad (9)$$

The BCP contains negative $\nabla^2\rho(r)$ to signify the stored potential energy, showing that the electronic charge is focused in the area between the nuclei, dividing it into two nuclei. This occurs in all covalent bonds where electrons are shared.

A positive Laplacian value, $\nabla^2\rho(r)$, at a bond critical point means that the local kinetic energy density outweighs the potential energy density, resulting in a depletion of electron density along the bond path, a hallmark of closed-shell electrostatic interactions. Conversely, a negative $\nabla^2\rho(r)$ at a BCP signifies a covalent bond, while a positive $\nabla^2\rho(r)$ indicates a closed-shell interaction, as found in van der Waals complexes, hydrogen bonds, and ionic bonds [77].

The local sign of the electronic energy density $H(r)$ at a bond critical point reflects the balance between kinetic and potential energy contributions: When $H(r) < 0$, potential-energy stabilization from electron accumulation dominates, as in covalent bonds. Koch and Popelier's scheme [76] further classifies interactions by both the Laplacian $\nabla^2\rho(r)$ and $H(r)$: Weak to moderate (closed-shell) interactions exhibit $\nabla^2\rho(r) > 0$ and $H(r) > 0$; stronger, partially shared-shell bonds show $\nabla^2\rho(r) > 0$ but $H(r) < 0$; and truly shared-shell (very strong) bonds are characterized by both $\nabla^2\rho(r) < 0$ and $H(r) < 0$. This classification implies a continuum where weak interactions gradually blend into weaker van der Waals forces, whereas strong bonds connect to covalent and polar bonds at the opposite end of the spectrum. In this study, NBO [71, 78] and QTAIM analyses were conducted on the optimized structures to elucidate the characteristics of the chemical bonds. The quantum theory of atoms in molecules (QTAIM) was applied using the AIM2000 software [79].

3. Results and discussion

3.1 B40 and encapsulated B40 fullerenes

Figure 1 displays the stable configurations of both bare and M@B40 (M = Mg and K) fullerenes, along with the corresponding TDOS plots. Table 1 provides a comprehensive list of the formation energy (E_{form}), NBO charges of B26 and B10 atoms (Q), energies of LUMO (E_{LUMO}) and HOMO (E_{HOMO}) the gaps between them (H-L gap) and dipole moments (μ) in both of gas and water media for these systems. The geometric configurations of bare B40 and M@B40 (M = Na and K) fullerenes were analysed, and it was found that the addition of magnesium and potassium elements does not change the structure of B40. The distance between the metal (magnesium or potassium) and the boron atom in the fullerene cage shows that the potassium atom tends more than magnesium to be placed in the center of the nanocavity, while the magnesium atom is away from the center and tends to be placed at the bottom of the cavity. It seems that the reason for this orientation is related to the size of the atomic radius of these metals. Potassium and magnesium are among the two groups of alkaline and alkaline earth elements [51], but they both belong to the third period of the periodic table. The atomic radius of magnesium is smaller than that of potassium, so the latter can transfer more charge than potassium and place the electron in the electron-deficient hole [43, 51]. This causes magnesium to pull towards the bottom of the hole center. The Mg@B40 and K@B40 systems exhibit encapsulated energy values of −1.9 and −0.68 eV, respectively. Consequently, it can be inferred that both systems are thermodynamically stable. The HOMO energy for M@B40 fullerenes is smaller (less negative)

https://dx.doi.org/10.57647/j.ijnd.2026.1701.06

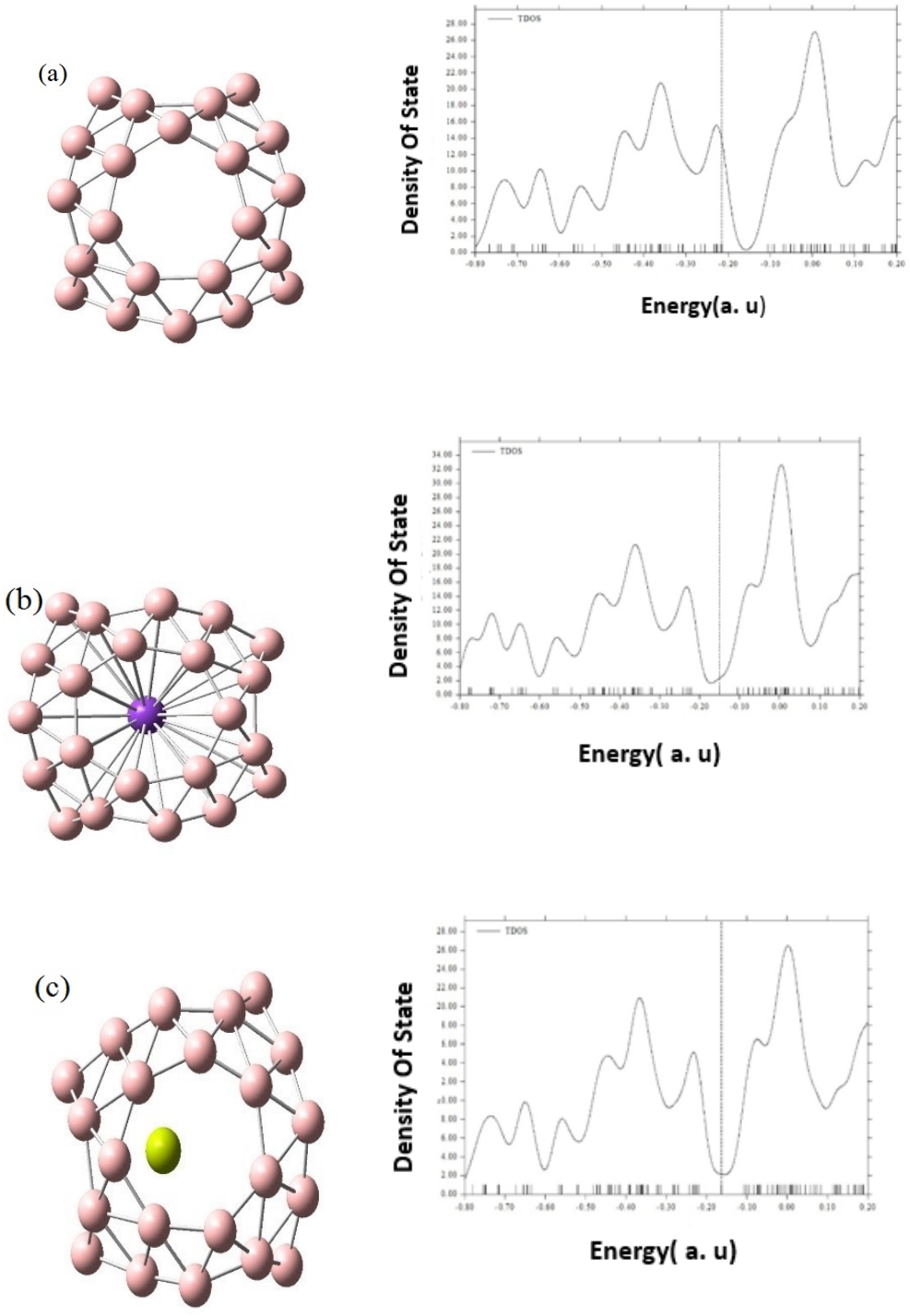

Figure 1. Optimized geometries (left) and total density of states (TDOS) spectra (right) for (a) pristine B40, (b) K@B40, and (c) Mg@B40. In each TDOS plot, the dashed line denotes the Fermi level.

compared to pure B40 fullerene, which exhibits that these structures are more interested in reacting with electrophilic species. Also, in most cases, the LUMO energy of M@B40 fullerenes are at a lower energy level contrasted to pure B40 fullerene, which again indicates the high tendency of these compounds to perform a chemical reaction compared to pure B40 fullerene.

According to Table 1, the HOMO and LUMO energy difference for the B40 structure in the gaseous and aqueous phases are reported as 2.93 eV. It is observed that the energy gap in all enclosed structures is reduced in comparison to pure fullerene, indicating that M@B40 structures exhibit lower kinetic stability than pure B40, making them more reactive. Moreover, as shown in Table 1, both the LUMO and HOMO levels decrease in the aqueous environment compared to the gas phase, reflecting destabilization of these frontier orbitals.

Table 1. Formation energies (E_{form}, eV), LUMO (E_{LUMO}, eV), HOMO (E_{HOMO}, eV), energy gaps (H-Lgap, eV), NBO charge of B26 and B10 atoms (Q, e), dipole moment (μ, Debye) of B40, Mg@B40, K@B40 fullerenes.

Parameter	Phase	B40	Mg@B40	K@B40
E_{form}		-	−1.9	−0.67
Q (B26 and B10)	Gas	0.075, −0.15	0.006, −0.043	0.059, −0.12
	water	0.08, −0.16	0.007, −0.13	0.06, −0.13
μ	Gas	0.004	0.30	0.0026
	water	0.0031	2.59	0.0073
E_{HOMO}	Gas	−5.83	−4.43	−4.21
	Water	−5.77	−4.19	−4.08
E_{LUMO}	Gas	−2.90	−2.93	−2.85
	Water	−2.83	−2.73	-2.81
H-L gap	Gas	2.93	1.50	1.36
	Water	2.93	1.46	1.27

3.2 β-Lap adsorption of pure and M@B40 (M = K and Mg) fullerene

Once acquainted with the electronic structure and surface reactivity of M@B40, the subsequent inquiry arises as to whether these altered fullerenes possess the capability to adsorb a β-Lap molecule. To identify the most stable β-Lap/B40 complex, a thorough investigation is conducted on several potential initial structures. To achieve this objective, the β-Lap molecule interacts with various locations on the fullerene structure, like a top the boron atom, heptagon, hexagon, and different B-B bonds, using its oxygen atoms in both vertical and horizontal orientations. The oxygen atoms (O_1, and O_2 in figure 2) form a bond with the boron atoms, figure 2 illustrates the maps depicting the molecular electrostatic potential (MEP), LUMO, and HOMO of β-Lap molecule. The HOMO, characterized by its electron-rich nature, is localized on the oxygen atoms of the drug [59]. As a result of a lack of electrons of the boron, it is expected that the nanocage will directly bind two B atoms to the oxygen atoms of β-Lap. Consequently, the interaction between β-Lap and the B40 fullerene can be characterized as an interaction between acid and base Lewis. The geometry optimization has been conducted, resulting in the identification of a stable complex as shown in figure 3.

In the complexes under consideration, the binding distance B-O followed the sequence: B40 > M@B40. Although shorter bond lengths suggest stronger interactions, evaluating complex stability ultimately hinges on adsorption energy as the principal metric. Table 2 exhibited the binding energies, changes in Gibbs free and enthalpy energies, in gas phase. Results demonstrated that the encapsulation of Mg and K led to an increase in the adsorption energy. The E_{ads} of β-Lap on metal encapsulated B40 have increased by 6-10 times respectively compared to bare B40. These outcomes suggest a regardable interaction between M@B40 in the gas phase. The fact that both the Gibbs free-energy change and the enthalpy change are negative indicates that drug adsorption onto these nanostructures is thermodynamically spontaneous and exothermic process under ambient (298.15 K) conditions (Table 2).

The TDOS diagrams of β-Lap-fullerene interaction show precious insight into the quiddity of the adsorption process (figure 3). The adsorption of β-Lap markedly alters the electronic properties of the systems. While grafting β-Lap onto pristine B40 has little effect on the fullerene's states near the Fermi level, its interaction with Mg- and K-encapsulated B40 induces substantial electron transfer from the cage to the drug. This charge redistribution lowers the β-Lap LUMO energy and narrows the HOMO–LUMO gap of both Mg@B40 and K@B40, which in turn enhances their electrical conductivity (σ) according to equation (10) [80]:

$$\sigma \propto \exp(-E_g/KT) \tag{10}$$

where E_g denotes the energy gap, K represents the Boltzmann constant, and T is the temperature, taken as 298.15 K. Thus M@B40 are expected to exhibit higher sensitivity to β-Lap compared to B40. Figure 4 exhibit the HOMO and LUMO isosurfaces of β-Lap/fullerene complexes.

3.3 Solvent effect

Furthermore, we explored the impact of solvents on the drug delivery process, recognizing their significance. Given that water is a prevalent biological molecule, we selected it as the solvent. Our approach involved utilizing the PCM [81] to refine the most stable configuration of the studied structures. To quantify solvent influence, we introduced the solvation energy (E_{solv}), which is calculated as the difference between the adsorption energy in an aqueous environment (E_{hyd}) and the adsorption energy in the gas phase (E_{ads}):

$$E_{solv} = E_{hyd} - E_{ads} \tag{11}$$

https://dx.doi.org/10.57647/j.ijnd.2026.1701.06

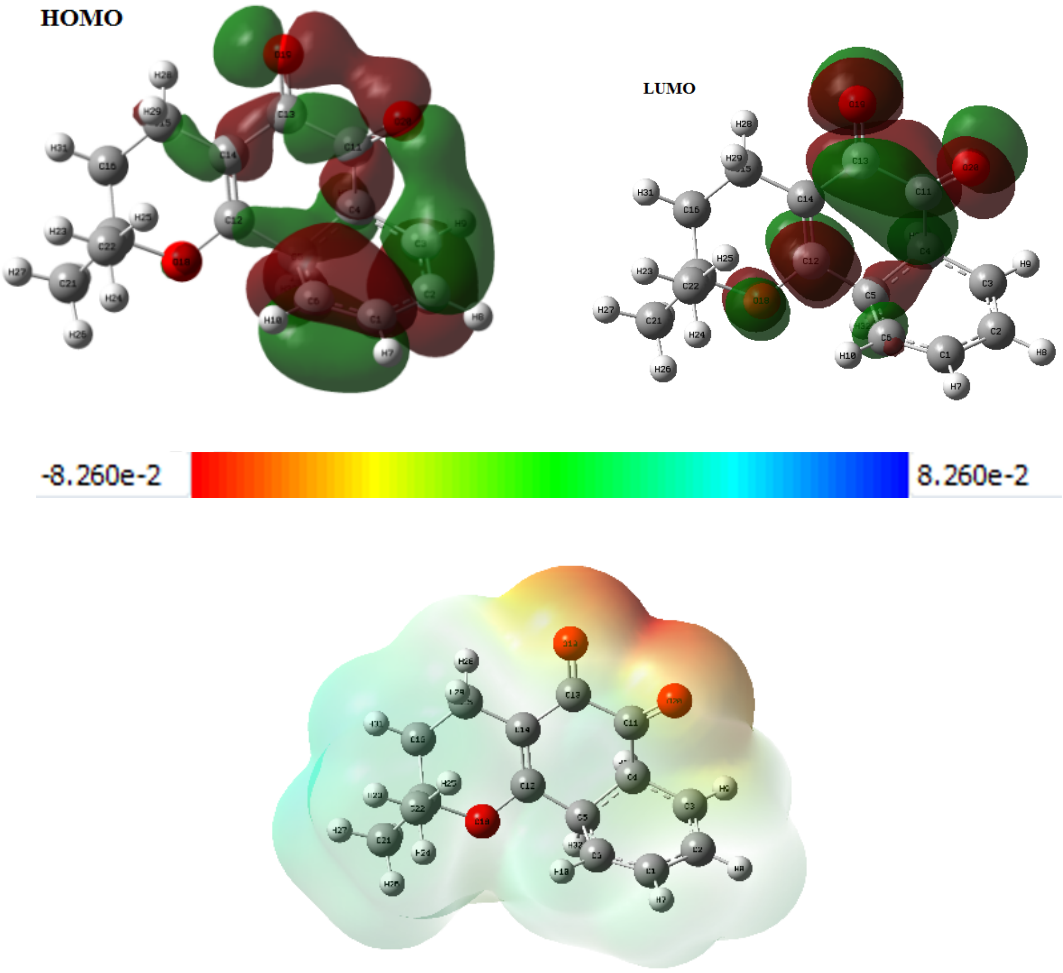

Figure 2. Frontier molecular orbitals and the MEP map of β-Lap.

Table 3 shows the E_{solv} for the β-Lap/fullerenes complexes. We also examined the adsorption energies (E_{hyd}), enthalpy changes (ΔH_{hyd}), and Gibbs free energy changes (ΔG_{hyd}) of these complexes when solvent molecules are present. The negative E_{solv} values in Table 3 demonstrate that all complexes are stabilized in water. However, solvent effects stabilize the individual components (β-Lap and fullerenes) more than the β-Lap–fullerene complexes themselves, leading to lower adsorption energies for the β-Lap molecule in solution compared to the gas phase. According to the fact that water is a polar solvent, the more polar complexes are to be more stable in this solvent. Dipole moments are essential considerations when designing drug delivery systems for biological applications. Tables 2 and 3 provides the calculated electronic dipole moment (μ) values for the investigated complexes in both gas and water phases. The dipole moment of the bare B40 fullerene is negligible in both gas and solution phases. However, after the creation of the β-Lap/B40 complex, the dipole moment increases significantly. This complex has a dipole moment of 9.58 Debye in the gas phase and 10.69 Debye in the water phase respectively. On the other hand, β-Lap/Mg@B40 and β-Lap/K@B40 have a dipole moment of 3.15 and 8.74 Debye in the gas media and 7.05 and 14.57 Debye in the water media respectively. The above results show that the dipole moment of M@B40 fullerene/drug complexes has increased up to two times in the aqueous environment compared to the gas media. This increase in dipole moment greatly enhances the solubility of these complexes in polar solvents, particularly water. Therewith, the increased hydrophilicity resulting from complex formation facilitates the movement of the drug within a alive system.

A crucial consideration is the subsequent desorption of the drug from the M-encapsulated B40 fullerene surface following its adsorption. The concentration of H_3O^+ is great owing to the redundant lactic production (pH < 7). The process of drug desorption within the acidic microenvironment of cancer cells can be investigated using a pH-dependent drug release mechanism.

An acidic environment (pH < 7) was used to promote protonation of the adsorbed β-lapachone on the M@B40 surfaces. To assess how protonation affects these com-

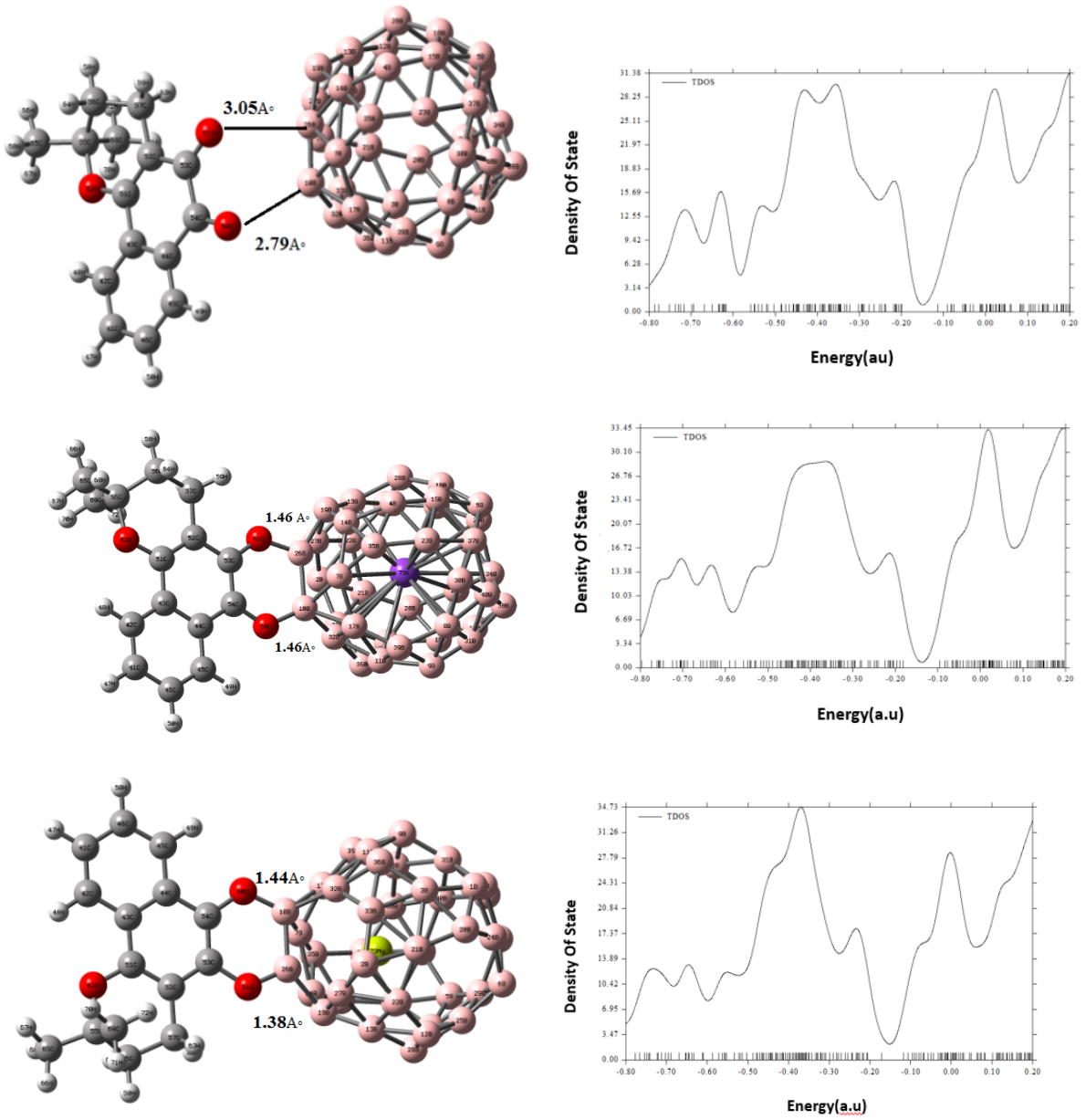

Figure 3. Optimized geometries (left) and TDOS spectra (right) for β-Lap adsorbed onto (a) B40, (b) K@B40 and (c) Mg@B40 (left).

plexes, we first identified the boron-bound oxygen sites on the B40 cage and added protons to those atoms, generating dicationic protonated adducts. These species were then fully geometry-optimized, and their protonation energies (E_{prot}) were obtained using the relation:

$$E_{prot} = (E_{[\beta-Lap-2H@M\text{-}B40]^{2+}} + 2E_{H_2O}) - (E_{\beta-Lap@M\text{-}B40} - 2E_{H_3O^+}) \quad (12)$$

Table 2. Adsorption energies (E_{ads}, kcal/mol), Gibbs free energy changes (ΔG_{ads}, kcal/mol) and enthalpy changes (ΔH_{ads}, kcal/mol) due to adsorption of β-Lap at room temperature and dipole moment (μ, Debye) of β-Lap-fullerene complexes within the gas phase.

Parameter	B40	Mg@B40	K@B40
E_{ads}	−5.5	−90	−62
ΔH_{ads}	−6.1	−91.3	−63.4
ΔG_{ads}	−6.6	−77	−49
μ	9.58	3.15	8.74

Table 3. Solvation energy (E_{solv}), Gibbs energy changes (ΔG_{hyd}) adsorption energy (E_{ads}), enthalpy changes (ΔH_{hyd}), all in kcal/mol and dipole moment (μ, Debye) of β-Lap/fullerene complexes within the water solvent.

Parameter	B40	Mg@B40	K@B40
E_{solv}	−0.3	−7.1	−7.7
E_{ads}	−5.2	−82.9	−55.7
ΔH_{hyd}	−5.9	−83.6	−59.3
ΔG_{hyd}	−8.7	−68.2	−44.04
μ	10.69	7.05	14.57

https://dx.doi.org/10.57647/j.ijnd.2026.1701.06

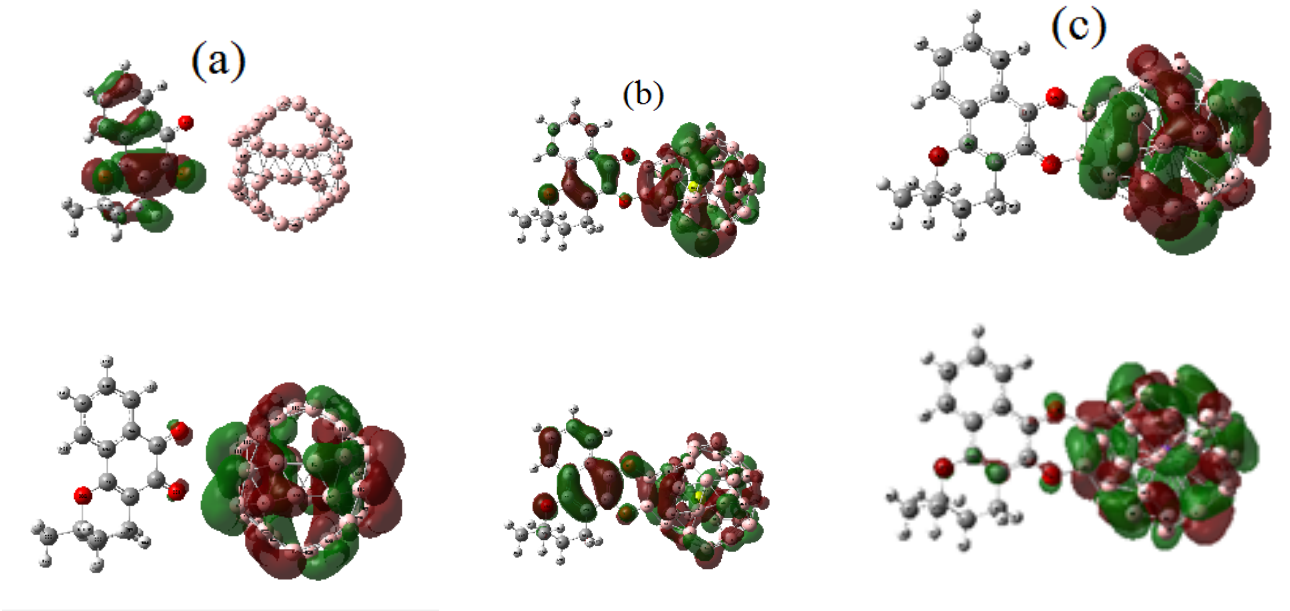

Figure 4. HOMO and LUMO isosurfaces of (a) β-Lap/B40, (b) β-Lap/Mg@B40 and (c) β-Lap/K@B4.

It is assumed that the oxygens of β-lap, bonded to the B atoms, are protonated. The protonation energies are −102.2 and −98.58 kcal/mol for K@B40 and Mg@B40, respectively. These remarkable negative protonation energies indicate that protonation occurs spontaneously in an acidic medium. Figure 5 also exhibits the optimized structures of protonated complexes including the O-B interaction distances. The O-B distances considered elongate upon protonation. The protonation of the β-Lap@K-B40 elongates the O-B bonds from 1.47 Å to 1.70 Å. Also, these bonds elongate from 1.45 Å to 1.60 Å in the case of β-Lap@Mg-B40. Thus, the strength interaction of the drug with the encapsulated cage decreases in an acidic medium and the drug can be easily released.

3.4 Atoms in molecules analysis

Tables 4 and 5 present for the gas- and solution-phase systems, the bond-critical-point of various B–O bonds, including the electron density $\rho(r)$, its Laplacian $\nabla^2\rho(r)$, the total electronic energy density $H(r)$, the kinetic energy density $G(r)$, and the potential energy density $V(r)$ for B40 and metal-encapsulated complexes with β-Lap in gas and solution phases. The $\rho(r)$ in BCP has frequently been demonstrated to be a good measure of bond strength. In accordance with these guidelines, the value of $\rho(r)$ ranges from 0.002 to 0.035 a.u. for weakly interacting systems. In agostic systems, the $\rho(r)$ lies outside the aforementioned interval. Moreover, the Laplacian $\nabla^2\rho(r)$ serves to differentiate interaction strength: values from 0.024 to 0.139 a.u. correspond to weak contacts, while those between 0.150 and 0.250 a.u. are characteristic of agostic bonds.

Inspection of Tables 4 and 5 reveals that, for every complex examined, the B–O bond electron density values extend beyond these defined limits, indicating that a covalent character is attributed to these interactions. In other words, in the case of anchor bonds (B-O), a positive value of $\nabla^2\rho(r)$ indicates a decrease in electronic charge along the bond length, indicating a closed shell electrostatic interaction. Tables 4 and 5 show that $H(r)$ at each B–O anchor bond is negative for every complex, signifying a stabilizing influence arising from the accumulated electron density in the bond region and the covalent character of these interactions. Therefore, the $\nabla^2\rho(r) > 0$ for B-O bond and the $H(r) < 0$ exhibit that the adsorption of β-Lap on the fullerenes is an electrostatic interaction in both gas and solution phases.

The $\rho(r)$ of the C54–O60 and C53–N61 bonds in β-Lap showed a reduction after being adsorbed onto the fullerenes. Greater interaction strength results in decreased $\rho(r)$ values for these bonds. It is important to mention that the $\rho(r)$ for the B-O bonds in β-Lap/Mg@B40 complex surpasses that of β-Lap/k@B40 and β-Lap/B40 complexes, highlighting the superior strength of the anchor bond in the β-Lap/Mg@B40 compared to the others.

As mentioned earlier, $H(r)$ is negative for all B-O bonds. This value is more negative for the B26–bond in the β-Lap/Mg@B40 than for this bond in the other complexes, indicating an increased covalent character of the B26–O61 bond in β-Lap/Mg@B40 compared to β-Lap/k@B40 and β-Lap/B40 complexes.

3.5 Natural bond orbital analysis

These calculations were carried out to elucidate the bonding interactions anchoring β-Lap to both pristine B40 and metal-encapsulated (Mg@B40 and K@B40) fullerenes, as well as to quantify the accompanying charge transfer. In B-O anchor bonds, electron donation occurs from the oxygen lone-pair orbitals into the boron antibonding (n*) orbitals. Because the three lone pairs on oxygen are differently oriented relative to these n* orbitals, they participate in the complex to varying degrees.

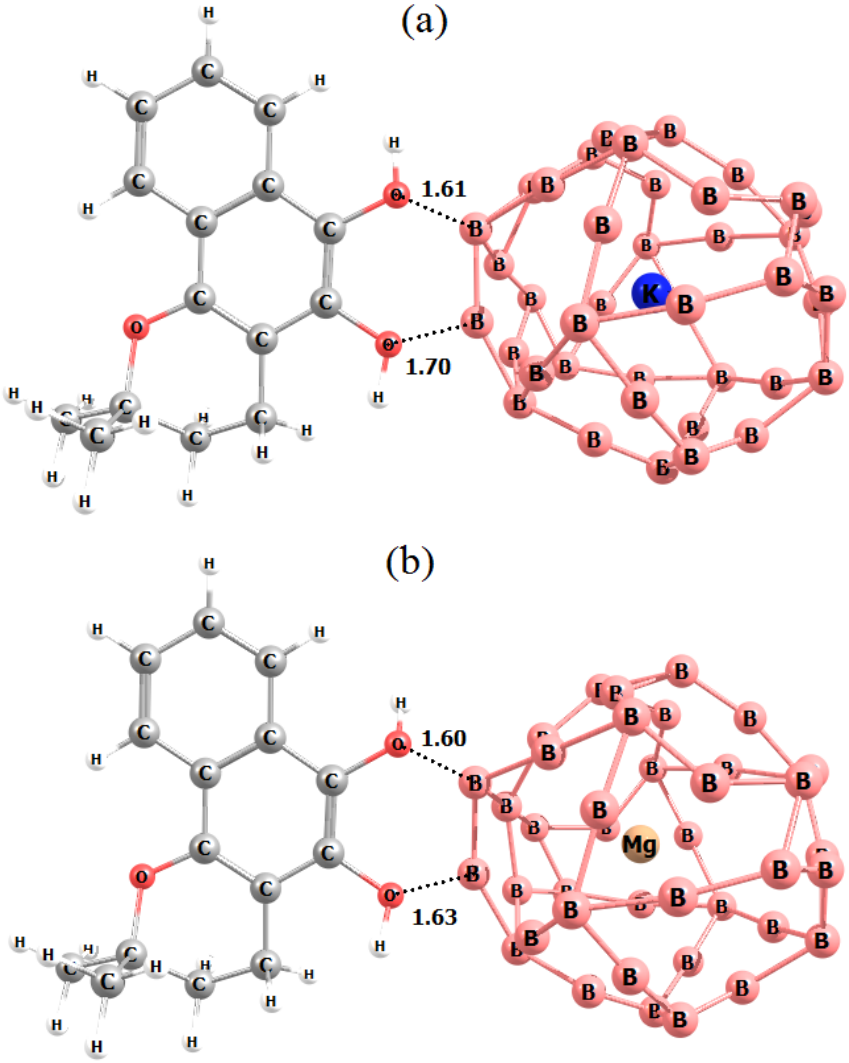

Figure 5. The optimized structures of the protonated complexes. (a) β-Lap/k@B40 and (b) β-Lap/Mg@B40.

Table 4. QTAIM topological parameters (in a.u.) of β-Lap-fullerene complexes (in Gas phase).

Complex	BCP	$\rho(r)$	$\nabla^2\rho(r)$	$G(r)$	$H(r)$	$V(r)$
β-Lap/B40	C54-O60	0.400	1.062	0.737	−1.409	0.671
	B10-O60	0.012	0.111	0.007	−0.008	0.000
	C53-O61	0.395	0.697	0.708	−1.372	0.664
	B26-O617 0.008	0.095	0.005	−0.005	−0.001	
β-Lap/k@B40	C54-O60	0.310	−0.640	0.448	−0.936	0.488
	B10-O60	0.151	2.954	0.273	−0.361	0.088
	C53-O61	0.304	−1.046	0.412	−0.888	0.477
	B26-O61	0.153	2.796	0.268	−0.362	0.093
β-Lap/Mg@B40	C54-O60	0.286	−1.365	0.351	−0.787	0.436
	B10-O60	0.166	3.057	0.296	−0.401	0.105
	C53-O61	0.266	−1.116	0.322	−0.714	0.392
	B26-O61	0.193	3.912	0.371	−0.497	0.126

https://dx.doi.org/10.57647/j.ijnd.2026.1701.06

Table 5. QTAIM topological parameters (in a.u.) of β-Lap-fullerene complexes (in Solution phase).

Complex	BCP	$\rho(r)$	$\nabla^2\rho(r)$	$G(r)$	$H(r)$	$V(r)$
β-Lap/B40	C54-O60	0.396	1.014	0.727	−1.391	0.664
	B10-O60	0.010	0.091	0.006	−0.006	0.000
	C53-O61	0.390	0.558	0.687	−1.340	0.652
	B26-O61	0.006	0.072	0.004	−0.003	−0.001
β-Lap/k@B40	C54-O60	0.314	−0.602	0.459	−0.956	0.497
	B10-O60	0.146	2.787	0.260	−0.345	0.086
	C53-O61	0.304	−1.082	0.409	−0.886	0.477
	B26-O61	0.152	2.753	0.265	−0.359	0.093
β-Lap/Mg@B40	C54-O60	0.286	−1.475	0.344	−0.779	0.436
	B10-O60	0.162	2.928	0.285	−0.386	0.102
	C53-O61	0.270	−1.228	0.325	−0.726	0.401
	B26-O61	0.1887	3.734	0.355	−0.477	0.122

In the Table 6, the ΔE_{CT} values between donor and acceptor orbitals in β-Lap complexes with B40 and metal-encapsulated are listed.

Overall, complexes characterized by lower orbital interaction (second-order perturbation) energies exhibit minimal charge transfer and thus display a predominantly ionic bonding character between the nanocage and the β-Lap molecule. As can be seen in Table 6, in all β-Lap complexes with B40 and metal-encapsulated, the interaction nO → n*B participates in the stabilization interaction. The most pronounced nO → n*B charge-transfer interaction occurs in the β-Lap/Mg@B40 complex, with ΔE_{CT} values of 501.35 kcal/mol in the gas phase and 492.03 kcal/mol in aqueous media. Additionally, Natural Population Analysis (NPA) calculations were performed to evaluate atomic charges and electron distribution patterns. The charge distributions of β-Lap/Mg@B40 active sites during interaction with B40 and metal-encapsulated are summarized in the Table 7. In the majority of complexes connected by B–O bonds, boron bears a positive partial charge while oxygen is partially negative, indicating electrostatic B–O interactions as confirmed by the QTAIM analysis.

Table 7. Calculated NPA charges of β-Lap-fullerene complexes.

Complex	bond type	q_O	q_B
β-Lap/B40	B10-O60	−0.436	−0.009
	B26-O61	−0.472	0.105
β-Lap/k@B40	B10-O60	−0.482	0.219
	B26-O61	−0.518	0.295
β-Lap/Mg@B40	B10-O60	−0.541	0.339
	B26-O61	−0.488	0.254

Comparison of B10-O60 and B26-O61 bonds in β-Lap/Mg@B40, β-Lap/k@B40 and β-Lap/B40 complexes shows that these bonds are stronger in β-Lap/Mg@B40 other complexes. Therefore, the electron density values in BCPs, total charge transfer energies, and ΔE_{CT} for B-O bonds in β-Lap/Mg@B40 complex are higher than β-Lap/k@B40 and β-Lap/B40 complexes.

Table 6. NBO charge transfer features of β-Lap-fullerene complexes.

Complexes	Interaction	ΔE_{CT}	Complexes	Interaction	ΔE_{CT}
Gas Phase			Solution Phase		
β-Lap/B40	nO60 → n*B10	6.87	β-Lap/B40	nO60 → n*B10	0.81
	nO61 → n*B26	2.48		nO61 → n*B26	1.01
β-Lap/k@B40	nO60 → n*B10	217.27	β-Lap/k@B40	nO60 → n*B10	214.70
	nO61 → n*B26	221.50		nO61 → n*B26	214.47
β-Lap/Mg@B40	nO60 → n*B10	501.35	β-Lap/Mg@B40	nO60 → n*B10	491.18
	nO61 → n*B26	500.73		nO61 → n*B26	492.03

https://dx.doi.org/10.57647/j.ijnd.2026.1701.06

4. Conclusion

In this research, interaction between β-Lap and B40 fullerenes were examined by DFT calculation. The yields revealed that β-Lap interacts with M@B40 (M = Mg and K) fullerenes compared to pristine B40 fullerene in both phases. Encapsulated complexes exhibited markedly increased dipole moments in aqueous solution compared to their gas-phase values. Also, the results show that solvent effect reduces adsorbed energy and ΔG_{ads}. Examining drug desorption for encapsulated fullerenes in cancer cells reveals that the drug release may occur simply within the cancer cells when protonation occurs, as pH-dependence. The electron density values in BCPs, total charge transfer energies, and ΔE_{CT} for B-O bonds in β-Lap/Mg@B40 complex are higher than β-Lap/k@B40 and β-Lap/B40 complexes. Based on these findings the B40 and M@B40 (M = Mg and K) may be viewed as promising delivery vehicles for the β-lap anticancer drug.

Authors contributions
Authors have contributed equally in preparing and writing the manuscript.

Availability of data and materials
The authors declare that the data supporting the findings of this study are available within the paper.

Conflict of interests
The authors assert that they do not have any identifiable conflicting financial interests or personal relationships that might be perceived to influence the work presented in this paper.

References

1. Alotaibi BS, Buabeid M, Ibrahim NA, Kharaba ZJ, Ijaz M, and Noreen S. "Potential of nanocarrier-based drug delivery systems for brain targeting: A current review of literature." International Journal of Nanomedicine 2021; 7517-33. DOI: 10.2147/IJN.S333657
2. Chow EKH and Ho D. "Cancer nanomedicine: from drug delivery to imaging." Science Translational Medicine 2013; 5:216rv4–rv4. DOI: 10.1126/scitranslmed.3005872
3. Ardekani ZM, Lorenzo-Leal AL, and Bach H. "Nanomedicine-mediated drug delivery for potential treatment of inflammatory bowel disease: a narrative review." Nanomedicine 2024; 19:163–79. DOI: 10.2217/nnm-2023-0267
4. Bansal M, Kumar A, Malinee M, and Sharma TK. "Nanomedicine: Diagnosis, treatment, and potential prospects." Nanoscience in Medicine 2020; 1:297–331. Available from: https://www.springer.com/series/11480
5. Chhikara B, Kumar R, Rathi B, Krishnamoorthy S, and Kumar A. "Prospects of Applied Nanomedicine: potential clinical and (bio) medical inter ventions via nanoscale research advances." Journal of Materials NanoScience 2016; 3:50–6. Available from: http://pubs.iscience.in/appnanomed
6. Fang X, Cao J, and Shen A. "Advances in anti-breast cancer drugs and the application of nano-drug delivery systems in breast cancer therapy." Journal of Drug Delivery Science and Technology 2020; 57:101662. DOI: 10.1016/j.jddst.2020.101662
7. Garbayo E, Pascual-Gil S, Rodríguez-Nogales C, Saludas L, Mendoza A Estella-Hermoso de, and Blanco-Prieto MJ. "Nanomedicine and drug delivery systems in cancer and regenerative medicine." Wiley Interdisciplinary Reviews: Nanomedicine and Nanobiotechnology. 2020; 12:e1637. DOI: 10.1002/wnan.1637
8. Aal SA. "DFT study of the therapeutic potential of borospherene and metalloborospherenes as a new drug-delivery system for the 5-fluorouracil anticancer drug." Journal of Molecular Liquids 2022; 360:119457. DOI: 10.1016/j.molliq.2022.119457
9. Liu J, Li S, Wang J, Li N, Zhou J, and Chen H. "Application of nano drug delivery system (NDDS) in cancer therapy: A perspective." Recent Patents on Anti-Cancer Drug Discovery 2023; 18:125–32. DOI: 10.2174/1574892817666220713150521
10. Zhang L, Zhang JC, Shi LF, Cheng X, Chen JH, and Sun WM. "On the possibility of using the Ti@Si16 superatom as a novel drug delivery carrier for different drugs: A DFT study." Journal of Molecular Graphics and Modelling 2023; 118:108378. DOI: 10.1016/j.jmgm.2022.108378
11. Lu S, Zhang C, Wang J, Zhao L, and Li G. "Research progress in nano-drug delivery systems based on the characteristics of the liver cancer microenvironment." Biomedicine & Pharmacotherapy 2024; 170:116059. DOI: 10.1016/j.biopha.2023.116059
12. Shang S, Li X, Wang H, Zhou Y, Pang K, Li P, et al. "Targeted therapy of kidney disease with nanoparticle drug delivery materials." Bioactive Materials 2024; 37:206–21. DOI: 10.1016/j.bioactmat.2024.03.014
13. Yuan S and Hu Q. "Convergence of nanomedicine and neutrophils for drug delivery." Bioactive Materials 2024; 35:150–66. DOI: 10.1016/j.bioactmat.2024.01.022
14. Han X, Gong C, Yang Q, Zheng K, Wang Z, and Zhang W. "Biomimetic nano-drug delivery system: An emerging platform for promoting tumor treatment." International Journal of Nanomedicine 2024 :571–608. DOI: 10.2147/IJN.S442877

15. Rai M, Gade A, Gaikwad S, Marcato PD, and Durán N. "Biomedical applications of nanobiosensors: The state-of-the-art. " Journal of the Brazilian Chemical Society 2012; 23:14–24. DOI: 10.1590/S0103-50532012000100004
16. Kong H, Yi K, Mintz RL, Wang B, Xu Y, Lao YH, et al. "CRISPR/Cas detection with nanodevices: moving deeper into liquid biopsy." Chemical Communications 2024. DOI: 10.1039/D3CC05375J
17. Babu YS, Kumari N, and Maruthi M. "Nanodevices in neurological infections: an update. In: Recent Developments in Nanomaterial-based Sensing of Human Pathogens." 2024; Elsevier:51–67. DOI: 10.1016/B978-0-443-18574-8.00017-0
18. Azari B, Pourahmad A, Sadeghi B, and Mokhtary M. "Green synthesis of SiO_2 from Equisetnm arvense plant for synthesis of SiO_2/ZIF-8 MOF nanocomposite as photocatalyst." Journal of Coordination Chemistry 2023; 76:219–31. DOI: 10.1080/00958972.2023.2166408
19. Li Y, Huang F, Stang PJ, and Yin S. "upramolecular Coordination Complexes for Synergistic Cancer Therapy." Accounts of Chemical Research 2024; 57:1174–87. DOI: 10.1021/acs.accounts.4c00031
20. Ostovan A, Milowska KZ, and García-Cervera CJ. "A twist for tunable electronic and thermal transport properties of nanodevices." Nanoscale 2024; 16:7504–14. DOI: 10.1039/D4NR00058G
21. Pan H, Liu P, Zhao L, Pan Y, Mao M, Kroemer G, et al. "Immunogenic cell stress and death in the treatment of cancer." Seminars in Cell & Developmental Biology 2024. DOI: 10.1016/j.semcdb.2023.10.007
22. Victoir B, Croix C, Gouilleux F, and Prié G. "Targeted Therapeutic Strategies for the Treatment of Cancer." Cancers 2024; 16:461. DOI: 10.3390/cancers16020461
23. Wang H, Wang X, Zhang X, and Xu W. "The promising role of tumor-associated macrophages in the treatment of cancer. " Drug Resistance Updates 2024 :101041. DOI: 10.1016/j.drup.2023.101041
24. Weth FR, Hoggarth GB, Weth AF, Paterson E, White MP, Tan ST, et al. "Unlocking hidden potential: advancements, approaches, and obstacles in repurposing drugs for cancer therapy." British Journal of Cancer 2024; 130:703–15. DOI: 10.1038/s41416-023-02502-9
25. Zhang J, Gu J, Wang X, Ji C, Yu D, Wang M, et al. "Engineering and Targeting Neutrophils for Cancer Therapy." Advanced Materials 2024; 36:2310318. DOI: 10.1002/adma.202310318
26. Zheng M, Zhang J, Deng C, Chen L, Zhang H, Xin J, et al. "he collaborated assembly of hydrophobic curcumin and hydrophilic cyanine dye into nanocolloid for synergistic chemo-photothermal cancer therapy." Materials & Design 2024; 241:112900. DOI: 10.1016/j.matdes.2024.112900
27. Afzal F, Ayub AR, Arshed SM, Taj A, Nabat KY, Hamid H, et al. "A DFT-Based quantum analysis of Optimizing B3O3 as a Melphalan nanocarrier for cancer therapy." Computational and Theoretical Chemistry 2024; 1236:114582. DOI: 10.1016/j.comptc.2024.114582
28. Daldossi C, Perilli D, Ferraro L, and Di Valentin C. "Functionalizing TiO_2 Nanoparticles with Fluorescent Cyanine Dye for Photodynamic Therapy and Bioimaging: A DFT and TDDFT Study." Journal of Physical Chemistry C 2024; 128:2978–89. DOI: 10.1021/acs.jpcc.3c08298
29. Deb J, Kundu A, Garg N, Sarkar U, and Chakraborty B. "Copper decorated graphyne as a promising nanocarrier for cisplatin anti-cancer drug: A DFT study." Applied Surface Science 2023; 622:156885. DOI: 10.1016/j.apsusc.2023.156885
30. Galini M, Salehi M, Kubicki M, Bayat M, and Malekshah RE. "Synthesis, structural characterization, DFT and molecular simulation study of new zinc-Schiff base complex and its application as a precursor for preparation of ZnO nanoparticle." Journal of Molecular Structure 2020; 1207:127715. DOI: 10.1016/j.molstruc.2020.127715
31. Gunes BA, Kirlangic OF, Kilic M, Sunguroglu A, Ozgurtas T, Sezginer EK, et al. "Palladium Metal Nanocomposites Based on PEI-Functionalized Nitrogen-Doped Graphene Quantum Dots: Synthesis, Characterization, Density Functional Theory Modeling, and Cell Cycle Arrest Effects on Human Ovarian Cancer Cells." ACS omega. 2024; 9:13342–58. DOI: 10.1021/acsomega.3c10324
32. Guo C, Gao X, Wang Q, Song C, Yu H, Wang Q, et al. "Density Functional Theory and Raman Spectroscopy Studies of Adsorption Sites of Au Nanoparticles with Alectinib." Langmuir 2023; 39:19048–55. DOI: 10.1021/acs.langmuir.3c03241
33. Sadjadi MS, Sadeghi B, and Zare K. "Natural bond orbital (NBO) population analysis of cyclic thionylphosphazenes, [NSOX $(NPCl2)_2$]; X = F (1), X = Cl (2)." Journal of Molecular Structure: THEOCHEM 2007; 817:27–33. DOI: 10.1016/j.theochem.2007.04.015
34. Laban BB, Novaković M, Vasić-Anićijević D, Bondžić AM, and Nikezić AV. "A combined experimental and DFT study of metal core/indocyanine green shell hybrid nanoparticles." Spectrochimica Acta Part A: Molecular and Biomolecular Spectroscopy 2024; 309:123828. DOI: 10.1016/j.saa.2023.123828
35. Sohrabnezhad S, Pourahmad A, Sadjadi M, and Sadeghi B. "Nickel cobalt sulfide nanoparticles grown on AlMCM-41 molecular sieve." Physica E: Low-dimensional Systems and Nanostructures 2008; 40:684–8. DOI: 10.1016/j.physe.2007.09.081

36. Pan Y, Zhang Z, Cun JE, Fan X, Pan Q, Gao W, et al. "Oxidase-like manganese oxide nanoparticles: A mechanism of organic acids/aldehydes as electron acceptors and potential application in cancer therapy." Nanoscale 2024; 16:2860–7. DOI: 10.1039/D3NR05127G
37. Kaur H, Kaur J, and Kumar R. "A review on all boron fullerene (B40): A promising material for sensing and device applications." Materials Today: Proceedings 2022; 48:1095–102. DOI: 10.1016/j.matpr.2021.07.465
38. Camacho-Cristóbal JJ, Rexach J, and González-Fontes A. "Boron in plants: deficiency and toxicity." Journal of Integrative Plant Biology 2008; 50:1247–55. DOI: 10.1111/j.1744-7909.2008.00742.x
39. Zhai HJ, Zhao YF, Li WL, Chen Q, Bai H, Hu HS, et al. "Observation of an all-boron fullerene. " Nature chemistry. 2014; 6:727–31
40. Zhang L, Ye YL, Li XH, Chen JH, and Sun WM. "On the potential of all-boron fullerene B40 as a carrier for anti-cancer drug nitrosourea." Journal of Molecular Liquids 2021; 32:117533. DOI: 10.1016/j.molliq.2021.117533
41. Suliman M, Kzar MH, Juma AS, Ali IA, Yasin Y, Sayyid NH, et al. "B40 and SiB39 fullerenes enhance the physicochemical features of curcumin and effectively improve its anti-inflammatory and anti-cancer activities." Journal of Molecular Liquids 2024; 395:123816. DOI: 10.1016/j.molliq.2023.123816
42. Mussavi MS and Hosseini S. "DFT study on the potential of M@B40 (M = Mg and K) metalloborospherenes as nanocarrier for 6-Thioguanine anticancer drug." Journal of Molecular Liquids 2024; 395:123900. DOI: 10.1016/j.molliq.2023.123900
43. Shakerzadeh E. "Li@B40 and Na@B40 fullerenes serving as efficient carriers for anticancer nedaplatin drug: A quantum chemical study." Computational and Theoretical Chemistry 2021; 1202:113339. DOI: 10.1016/j.comptc.2021.113339
44. Aal SA. "Metalloborospherenes as a potential promising high drug-loading capacity for anticancer 5-fluorouracil drug: A DFT mechanistic approach." Computational and Theoretical Chemistry 2023; 1221:114046. DOI: 10.1016/j.comptc.2023.114046
45. Kosar N, Koudjina S, Ayub K, Gilani MA, Imran M, and Mahmood T. "Mechanistic enhanced cell voltage based on halides doped metal oxide fullerenes for use in Li-ion batteries: Insights from DFT intuition. " Diamond and Related Materials 2024; 142:110778. DOI: 10.1016/j.diamond.2023.110778
46. Vohra R, Kaur H, Kaur J, and Kumar R. "Investigation of transport behavior in borospherene-based molecular wire for rectification applications." Journal of Materials Research 2022 :1–9. DOI: 10.1557/s43578-021-00364
47. Shakerzadeh E. "Efficient carriers for anticancer 5-fluorouracil drug based on the bare and M-encapsulated (M = Na and Ca) B40 fullerenes; in silico investigation." Journal of Molecular Liquids 2021; 343:116970. DOI: 10.1016/j.molliq.2021.116970
48. Kaur H, Kaur J, and Kumar R. "Comparative study of symmetrical and asymmetrical B40 molecular junctions." Journal of Computational Electronics 2022; 21:599–607. DOI: 10.1007/s10825-022-01872-2
49. Shakerzadeh E. "Endohedral M@B40 (M = Na and Ca) metalloborospherenes as innovative potential carriers for chemotherapy melphalan drug: A theoretical study." Applied Organometallic Chemistry 2021; 35:e6411. DOI: 10.1002/aoc.6411
50. Fa W, Chen S, Pande S, and Zeng XC. "Stability of metal-encapsulating boron fullerene B40." Journal of Physical Chemistry A 2015; 119:11208–14. DOI: 10.1021/acs.jpca.5b07173
51. Bai H, Chen Q, Zhai HJ, and Li SD. "Endohedral and exohedral metalloborospherenes: M@B40 (M = Ca, Sr) and M@B40 (M = Be, Mg)." Angewandte Chemie International Edition 2015; 54:941–5. DOI: 10.1002/anie.201408738
52. Pardee AB, Li Y, and Li CJ. "Cancer therapy with β-lapachone." Current Cancer Drug Targets 2002; 2:227–42
53. Chen Y, Wu R, Li X, Cao M, Yang M, and Fu Bno. "β-Lapachone, an NQO1 bioactivatable drug, prevents lung tumorigenesis in mice." European Journal of Pharmacology 2024; 973:176511. DOI: 10.1016/j.ejphar.2024.176511
54. de Moraes DC, Rollin-Pinheiro R, Pinto MCFR, Domingos LTS, Barreto-Bergter E, and Ferreira-Pereira A. "Antifungal activity of β-lapachone against a fluconazole-resistant Candida auris strain." Brazilian Journal of Microbiology 2024 :1–9. DOI: 10.1007/s42770-024-01375-1
55. Khosropour E, Hakimi L, Mirjalili A, and Alavian A. "Antimalarial Response, Traditional and Other Potential Uses of Tabebuia Genera. " 2023; Antimalarial Medicinal Plants: CRC Press:279–93. DOI: 10.1201/9781003378396-19
56. Nguyen HT, Pham-The H, Tuan AN, Thu HNT, Thi TAD, Le-Nhat-Thuy G, et al. "Improved synthesis, molecular modeling and anti-inflammatory activity of new fluorinated dihydrofurano-naphthoquinone compounds." Bioorganic & Medicinal Chemistry Letters 2024; 104:129714. DOI: 10.1016/j.bmcl.2024.129714

57. Qadir MI, Iqbal MS, and Khan R. "β-lapachone: A promising anticancer agent with a unique NQO1 specific apoptosis in pancreatic cancer. " Current Cancer Drug Targets 2022; 22:537–40. DOI: 10.2174/1568009622666220427121127
58. Lima KMM, Calandrini de Azevedo LF, Rissino JD, Vale VV, Costa EVS, Dolabela MF, et al. "Anticancer Potential and Safety Profile of β-Lapachone In Vitro." Molecules 2024; 29:1395
59. Gholami A, Shakerzadeh E, and Anota EC. "Exploring the potential use of pristine and metal-encapsulated B36N36 fullerenes in delivery of β-lapachone anticancer drug: DFT approach. " Polyhedron 2023; 232:116295. DOI: 10.1016/j.poly.2023.116295
60. Ning L, Jingling S, Jinhai S, Laishun L, Xiaoyu X, Meihong L, et al. "Study on the THz spectrum of methamphetamine." Optics Express 2005; 13:6750–5. DOI: 10.1364/OPEX.13.006750
61. Becke AD. "Perspective: Fifty years of density-functional theory in chemical physics. " Journal of Chemical Physics 2014; 140:61. DOI: 10.1063/1.4869598
62. Zhao Y and Truhlar DG. "Density functionals with broad applicability in chemistry." Accounts of Chemical Research 2008; 41:157–67. DOI: 10.1021/ar700111a
63. Frisch M. gaussian 09, Revision d. 01, Gaussian. Inc, Wallingford CT. 2009
64. Schuchardt KL, Didier BT, Elsethagen T, Sun L, Gurumoorthi V, Chase J, et al. "Basis set exchange: A community database for computational sciences." Journal of Chemical Information and Modeling 2007; 47:1045–52. DOI: 10.1021/ci600510j
65. Ri MH, Jang YM, Ri US, Yu CJ, Kim KI, and Kim SU. "Ab initio investigation of adsorption characteristics of bisphosphonates on hydroxyapatite (001) surface." Journal of Materials Science 2018; 53:4252–61. DOI: 10.1007/s10853-017-1880-1
66. Foresman J and Frish E. "Exploring chemistry." 1996; Gaussian Inc, Pittsburg, USA.
67. Bader RF. "Everyman's Derivation of the Theory of Atoms in Molecules." Journal of Physical Chemistry A 2007; 111:7966–72. DOI: 10.1021/jp073213k
68. Popelier P, Aicken F, and O'Brien S. " Atoms in molecules." 2000; 188:Manchester: Prentice Hall Manchester
69. Becke A. "The quantum theory of atoms in molecules: from solid state to DNA and drug design." 2007; John Wiley & Sons
70. Reed AE, Curtiss LA, and Weinhold F. "Intermolecular interactions from a natural bond orbital, donor-acceptor viewpoint." Chemical Reviews 1988; 88:899–926. DOI: 10.1021/cr00088a005
71. Reed AE and Weinhold F. "Natural bond orbital analysis of near-Hartree–Fock water dimer. " Journal of Chemical Physics 1983; 78:4066–73. DOI: 10.1063/1.445134
72. Reed AE and Weinhold F. "Natural localized molecular orbitals." Journal of Chemical Physics 1985; 83:1736–40. DOI: 10.1063/1.449360
73. Reed AE, Weinstock RB, and Weinhold F. "Deep learning-based artificial intelligence model for classification of vertebral compression fractures: A multicenter diagnostic study." Journal of Chemical Physics 1985; 83:735–46. DOI: 10.1063/1.449486
74. Foster JP and Weinhold F. "Natural hybrid orbitals." Journal of the American Chemical Society 1980; 102:7211–8. DOI: 10.1021/ja00544a007
75. Chocholoušová J, Špirko V, and Hobza P. "First local minimum of the formic acid dimer exhibits simultaneously red-shifted O–H. . .O and improper blue-shifted C–H. . .O hydrogen bonds." Physical Chemistry Chemical Physics 2004; 6:37–41. DOI: 10.1039/B314148A
76. Koch U and Popelier PL. "Characterization of CHO hydrogen bonds on the basis of the charge density." Journal of Physical Chemistry 1995; 99:9747–54. DOI: 10.1021/j100024a016
77. Bader RF. "A bond path: a universal indicator of bonded interactions." Journal of Physical Chemistry A 1998; 102:7314–23. DOI: 10.1021/jp981794v
78. Glendening E, Badenhoop J, Reed A, Carpenter J, Bohmann J, Morales C, et al. GEN NBO 5.0; Board of Regents of the University of Wisconsin System on behalf of the Theoretical Chemistry Institute: Madison, WI. 2001. DOI: 10.1021/jp2080226
79. Biegler-König F and Schönbohm J. "Update of the AIM2000-program for atoms in molecules. " Journal of Computational Chemistry 2002; 23:1489–94. DOI: 10.1002/jcc.10085
80. Li SS. "Semiconductor physical electronics." 2012; Springer Science & Business Media
81. Mennucci B and Tomasi J. "Continuum solvation models: A new approach to the problem of solute's charge distribution and cavity boundaries. " Journal of Chemical Physics 1997; 106:5151–8. DOI: 10.2147/IJN.S333657